Thermally conductive separator with hierarchical nano/microstructures for improving thermal management of batteries

Citation: Yang, Yuan et al. "Thermally Conductive Separator with Hierarchical Nano/microstructures for Improving Thermal Management of Batteries." Nano Energy 22 (April 2016): 301–309 © 2016 Elsevier Ltd

As Published: http://dx.doi.org/10.1016/j.nanoen.2016.01.026

Publisher: Elsevier

Persistent URL: http://hdl.handle.net/1721.1/114572

Version: Author's final manuscript: final author's manuscript post peer review, without publisher's formatting or copy editing

Thermally Conductive Separator with Hierarchical Nano/microstructures for Improving Thermal Management of Batteries

Yuan Yang[1,2*], Xiaopeng Huang[1], Zeyuan Cao[2], and Gang Chen[1*]

[1]Department of Mechanical Engineering, Massachusetts Institute of Technology, Cambridge, MA 02139, [2]Department of Applied Physics and Applied Mathematics, Columbia University, NY 10027

*Corresponding authors:

Gang Chen gchen2@mit.edu , Yuan Yang yy2664@columbia.edu

Abstract

Thermal management is critical to improving battery performance and suppressing thermal runaway. Besides developing external cooling technologies, it is important to understand and control thermal transport inside batteries. In this paper, heat transfer inside batteries is first analyzed and the thermal conductivity of each component is measured. The results show that low thermal conductivity of the separator is one major barrier for heat transfer in Li-ion batteries. To improve thermal conductivity of the separator, a hierarchical nano/micro-Al_2O_3/polymer separator is prepared with thermal conductivity of ~1 W $m^{-1}K^{-1}$, representing an enhancement of 5 X compared to commercial polyethylene-based separators. Modeling has been performed to understand mechanism behind the enhancement of thermal conductivity, which suggests that addition of nanoparticles significantly reduces thickness of polymer coating on micron-sized Al_2O_3 particles and thus increase the thermal conductivity of the composite separator. This Al_2O_3-based separator also has similar ionic conductivity with commercial polymer separators. Such composite separator may have potential applications in developing batteries with better performance and safety.

1. Introduction

High-performance batteries are important for various applications ranging from portable electronics, electric vehicles and grid-level energy storage.[1, 2] Thermal management of state-of-the-art Li-ion batteries (LIBs) and future higher energy batteries is critical to their performance and safety, especially at large scale.[3-6] The high temperature significantly deteriorates cycle life and it is one important reason to trigger

thermal runaway, especially for batteries with high energy and power density.[7-10] Past efforts mainly focus on modeling of external cooling technologies, such as forced air and liquid cooling, to lower battery temperature[5, 11-19], where the lumped heat transfer model is widely used without considering thermal conductivity (*k*) of a battery itself[15-18]. Only a few references took battery thermal conductivity into account with assumed values[5, 11, 19]. Improving thermal transport inside batteries can also facilitate heat dissipation, reduce temperature inhomogeneity and thermal stress in batteries. In this paper, we first measured thermal conductivity of different components in batteries and identified that the battery separator is a major limiting factor for heat dissipation in batteries. Then a thermally conductive Al_2O_3/polymer composite separator was developed to improve heat dissipation in batteries. The Al_2O_3/polymer hybrid separator contains both micron-sized and nano-sized Al_2O_3 particles as the thermally conductive phase, and Poly(vinylidene fluoride-hexafluoropropylene) (PVdF-HFP) as the binder. The large surface area of nanoparticles reduces thickness of polymer coating on Al_2O_3 and enhances thermal conductivity of the separator. At the optimized materials loading ratio, a thermal conductivity of 1.05 ± 0.16 W m^{-1} K^{-1} is reached, which is more than five times that of commercial polyethylene/polypropylene (PE/PP)-based commercial separator. Such separators could improve heat conduction and reduce the temperature rise of batteries in operations. Meanwhile, the composite separator shows similar ionic conductivity as commercial polyethylene-based separators, avoiding excessive joule heating due to slower ionic transport across the separator.

2. Materials and Methods

Materials. Micro-Al_2O_3 particles (~10 μm) were purchased from Sigma Aldrich. Kynar 2801 PVdF-HFP was received from Arkema. Commercial single-side coated $LiCoO_2$ and graphite electrodes, separators and nano-Al_2O_3 particles (~100 nm) were purchased from MTI Corporation. The Al_2O_3/PVdF-HFP composite separator was prepared by dispersing micro-Al_2O_3 particles, nano-Al_2O_3 particles and PVdF-HFP binders in THF for 12 hours and drop casting onto a flat glass substrate. A mold made of Aluminum is used to confine the dispersion and shape the separator to the desired dimension. The typical sample size is 3 cm by 3 cm. The weight ratio of PVdF-HFP to THF is fixed as 1:11. The ratio of PVdF-HFP to Al_2O_3 varies from 20 : 80 to 10 : 90. After drying, the Al_2O_3/PVdF-HFP film is peeled off from the glass substrate and pressed under 0.1 ton for 5 min at room temperature.

Cross-plane thermal conductivity measurement. The thermal conductivity is measured by stacking multiple electrode films together to ensure that thermal resistance of sample is one order of magnitude higher than the thermal contact resistance between copper and sample. After the environmental temperature is stabilized, the thermoelectric plate cools the bottom side of the sample while the heater is used to keep temperature of the top surface the same as the environment. The heater power (Q) is recorded after temperature is stabilized, indicated as the average power over 30 seconds after stabilization. Temperature data is recorded by K - type thermocouple. More details can be found in section 2 of the supporting information.

Ionic Conductivity Measurement. Ionic conductivity is measured by sandwiching the separator between two pieces of stainless steel with the same size and applying an AC voltage with amplitude of 10 mV at 50 kHz. The electrolyte is 1 M $LiClO_4$ in Ethylene carbonate/Diethyl carbonate (EC:DEC) with weight ratio of 1:1.

COMSOL Simulation. In simulation of temperature rise, external heat transfer coefficient is assumed to be 1000 W m^{-1} K^{-1} and 20 W m^{-1} K^{-1} for forced liquid cooling and force air cooling, respectively. The voltage loss due to internal resistance is supposed to be 0.6 V. The simulation time for 3C rate is 1200 s. The capacity of 18650 cell is set to 3.1 Ah. Liquid cooling is applied to all surfaces. For prismatic cells, the volumetric energy density is set to 600 Wh L^{-1} for the all cells. More details can be found in section 4 in the supporting information.

3. Results and Discussions

A typical Li-ion battery is made up of a triple-layer structure with a porous separator sandwiched between two composite electrodes (Figure 1a). The porous separator is typically made of polypropylene and polyethylene[20], while two electrodes are mixtures of active materials (e.g. $LiCoO_2$ or graphite, ~80-95 wt%), carbon black (2-10 wt%) and polymeric binder (1-10 wt%) (See figure S1 for SEM images of electrodes and separators). The triple-layer structure is assembled together to form either a roll in a cylindrical cell or a cuboid in a prismatic cell (Figure 1b). Voids in electrodes and separators are filled with carbonate-based organic electrolyte. In battery operation, heat is generated throughout the cell due to joule heat and entropy change in electrochemical

processes[21]. The heat produced is first conducted inside the cell through both in-plane and cross-plane directions of the triple-layer structure, followed by dissipation process outside the cell, such as air/liquid convection (Figure 1b). The in-plane direction of the triple-layer structure corresponds to the axial direction in cylindrical cells and width/length directions in prismatic cells with a thermal conductivity of $k_{//}$, while the cross-plane direction corresponds to the radial direction in cylindrical cells and thickness direction in prismatic cells with a thermal conductivity of $k_{\perp}$. To understand limiting factors for heat dissipation in batteries, thermal conductivity of battery components is measured first, followed by estimation of thermal resistance of different directions and external convection.

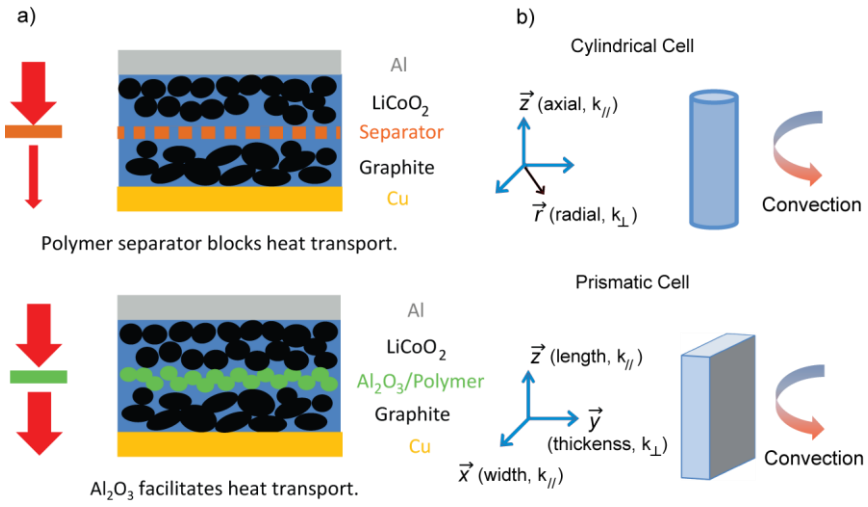

Figure 1. The structure of common Li-ion batteries and heat dissipation. (a) A typical Li-ion battery consists of three layers: composite cathode (e.g. $LiCoO_2$) with Al as the substrate, porous separator, and composite anode (e.g. graphite) with Cu as the substrate. The cross-plane heat transport is mainly limited by thermal resistance of the separator layer due to its low thermal conductivity. (b) Heat transfer in both in-plane and cross-plane directions of the triple-layer structure inside batteries, and then dissipate through convection outside batteries.

The first step in our analysis is to obtain thermal conductivity of electrodes and separators by experimental measurements. In the past, Maleki et al used laser flash method to measure $k_{\perp}$ and $k_{//}$ of electrodes and the triple-layer structure at different state-of-charge[22]. Their results show that $k_{\perp}$ of electrodes and trilayer are ~3 W m^{-1} K^{-1} when saturated with electrolyte, while $k_{//}$ is 20-30 W m^{-1} K^{-1}. However, a single-layer model is applied to multi-layer samples with distinct thermal properties in their study. In this report, $k_{\perp}$ of electrodes and separators are measured by a differential steady state method, as discussed in our previous work[23] (figure 2a), which uses heat flux applied to the sample, temperature difference across the sample and sample geometry to derive $k_{\perp}$ based on the Fourier's law. To reduce the effect of contact thermal resistance, multiple layers of battery electrodes or separators are stacked together so that the thermal resistance of sample (~1 X 10^{-3} m^2 K W^{-1}) is much larger than contact resistance between copper plates and the sample (~1 X 10^{-4} m^2 K W^{-1}). To mimic a real battery, we focus on electrodes and separators saturated with diethyl carbonate (DEC), one major component in LIB electrolyte. No salt is added since it contributes little to thermal conductivity[24] and it is sensitive to moisture. $k_{\perp}$ of $LiCoO_2$ electrode, graphite electrode and separators saturated with DEC are measured to be 1.06 ± 0.16, 2.0 ± 0.3, and 0.19 ± 0.03 W $m^{-1}K^{-1}$ (Table 1), which are in the same order of previous results by the laser flash method[22]. The in-plane thermal conductivities ($k_{//}$) of electrodes are dominated by metal substrates (Al for $LiCoO_2$ and Cu for graphite), so $k_{//}$ of electrodes are calculated based on the literature values[25] thermal conductivity of metals. $k_{//}$ of the separator is considered to be the same as $k_{\perp}$. Details of experimental procedures and calculations can be found in section 2 and 3 in the supporting information.

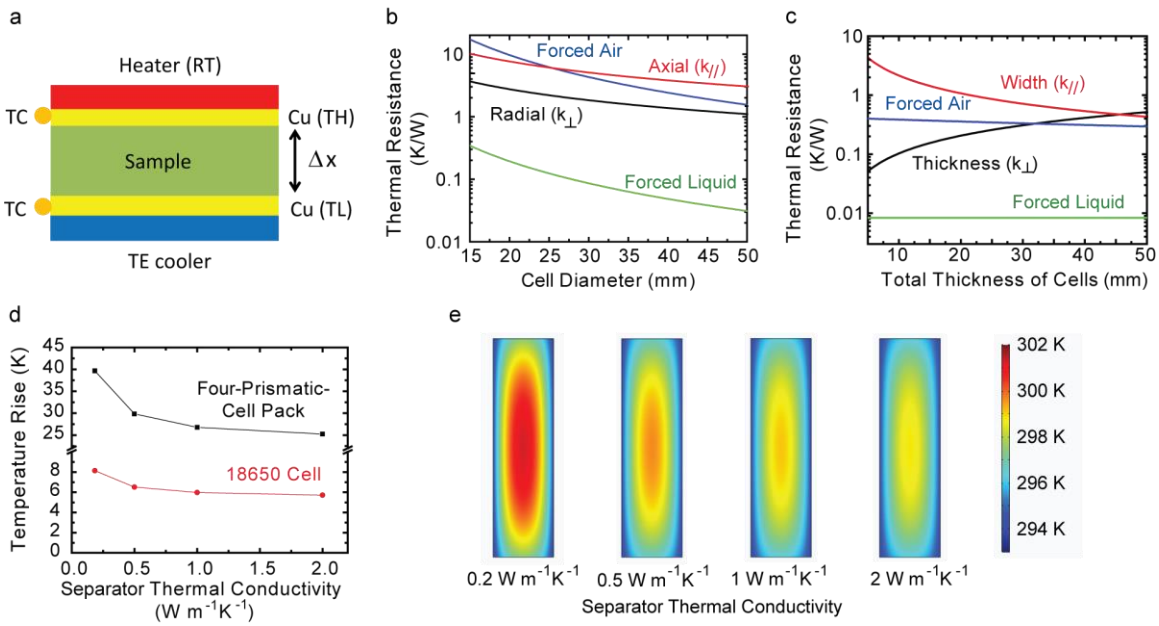

Figure 2. Measurements and simulations of heat transfer in Li-ion batteries. a) A schematic of the differential steady state method to measure thermal conductivity. A thermoelectric (TE) cooler cools the bottom side of a sample with a thickness of Δx while a thin film heater keeps top surface at the same temperature as the environment, which minimizes heat loss to the environment and improves accuracy of measured heat flux through the sample. Copper plates are used to realize uniform temperature distribution at two ends of the sample, which are measured by thermocouples (TCs). b) and c) Calculated thermal resistances of b) the cylindrical cell configuration and c) the prismatic cell configuration. The cylindrical cell dimension is scaled from an 18650 cell. The definition of directions in b) and c) is the same as figure 1b. Symbols in parenthesis indicate corresponding thermal conductivity in the direction. d) Numerical simulation by COMSOL Multiphysics on temperature rise against thermal conductivity of separator in a four-prismatic-cell pack and a 18650 cell, respectively. e) Corresponding temperature distribution in the cross section of an 18650 cell with the same simulation described in (d). The cross section passes the central axis of the cylindrical cell.

Table 1. Measured thermal properties of electrodes and separators in batteries

	Positive	Negative	Separator
Electrode Material	$LiCoO_2$	Graphite	PP/PE/PP
Substrate	15 μm Al	9 μm Cu	N/A
Thickness of Active Materials (μm)	82	106	24
Cross-plane Thermal Conductivity with DEC ($k_{\perp}$,W $m^{-1}K^{-1}$)*	2.0±0.3	1.06±0.16	0.19±0.03
Effective In-plane Thermal Conductivity ($k_{//}$,W $m^{-1}K^{-1}$)*	28	31	0.19±0.03

* With metal substrate taken into account for both positive and negative electrodes

The next step in our study is to estimate thermal resistance and heat generation/dissipation in batteries to understand the limiting factor. Two cell geometries are considered. One is the cylindrical cell scaled from 18650 cells with height of 65 mm and diameter of 18 mm, which means that the ratio of height to diameter is kept at 65/18. Another geometry is stacked prismatic cells where a single cell has two sides of 216 and 290 mm, respectively, and thickness of 7 mm. This dimension is the same as that used in Nissan leaf[26]. Thermal resistances along different directions are simply estimated based on one-dimensional heat conduction along the corresponding direction. It is defined as $\Delta T/Q$ at steady state with uniform heat generation inside the cell, where ΔT is the temperature difference between the center and surface of the cell, and Q is total heat transferred at cell surface. In calculation, the thermal conductivity along a direction in the cell is supposed to be the same as the effective thermal conductivity of the triple layer along the same direction, since the thickness of a triple layer (200-300 μm) is much smaller than the cell dimension (> 5 mm). The thermal resistance of external heat transfer

is estimated as $1/hA$, where h is the heat transfer coefficient, and A is the surface area for external convection.

Calculation results are shown as figure 2b and c for cylindrical and prismatic cell configuration, respectively. Although $k_{\perp}$ is much smaller than $k_{//}$ in batteries, the total thermal resistance along the cross-plane direction is actually smaller, as the cross-plane direction has larger cross sectional area and smaller length for heat transfer. This indicates that heat dissipation along the cross-plane direction is actually more efficient than in-plane. Regardless of cell geometry and dimension, thermal resistance of forced liquid cooling is much less than the cell, as h of liquid is very high, typically in the order of 1000 W m^{-2} K^{-1} [27], which indicates that heat dissipation is limited by the cell itself under forced liquid cooling. In the scenario of forced air cooling, thermal resistance of air convection is the limiting factor instead of heat conduction inside a cell, as h of forced convective air is only ~ 20 W m^{-2} K^{-1} [27]. Therefore, improving $k_{\perp}$ of the triple layer structure in batteries can effectively enhance total heat dissipation in batteries, especially when forced liquid cooling is used. Further analysis shows that the separator layer counts for 46% of total cross-plane thermal resistance of the triple-layer structure (section 3 in supporting information), while the $LiCo_2$ and graphite electrodes contribute 33% and 21%, respectively; thus the key to enhance heat dissipation is to increase the separator's cross-plane thermal conductivity ($k_{\perp,separator}$).

To further validate this argument, COMSOL simulation was carried out to understand the effect of $k_{\perp,separator}$ on temperature rise (T_{rise}) of a battery in operation. For example, Under 3C rate (charge or discharge in 1/3 hour) and forced liquid cooling, T_{rise} at the end of discharge in a four-prismatic-cell pack and a single 18650 cell

decreases from 40 ºC to 27 ºC and from 8 ºC to 6 ºC, respectively, when $k_{\perp,separator}$ increases from 0.185 W m^{-1} K^{-1} to 1 W m^{-1} K^{-1}. These values correspond to reduction of 33% and 25% in T_{rise}, respectively. Higher thermal conductivity of separator also leads to more uniform temperature distribution inside the cell, as illustrated in temperature distribution of the cell cross section (figure 2e and S4). The more uniform temperature distribution helps reduce performance degradation due to thermal stress. Further enhancement of $k_{separator}$ beyond 1 W m^{-1} K^{-1} does not significantly reduce T_{rise} or improve temperature homogeneity, as thermal resistance of electrodes begins to dominate. Therefore, 1 W m^{-1} K^{-1} is set as the target for thermally conductive separators. However, common polymers only have k of 0.2-0.5 W m^{-1} K^{-1} [15, 28]; thus pure polymer-based separators are difficult to achieve k of ~1 W m^{-1} K^{-1}, especially along the cross-plane direction. To address this challenge, we develop an inorganic/organic hybrid separator to realize high cross-plane thermal conductivity, where the inorganic phase, such as Al_2O_3, provides pathway for efficient heat transfer, as Al_2O_3 is of low cost and has high thermal conductivity of ~35 W m^{-1} K^{-1} [29], and the polymeric phase acts as binder to maintain integrity of the separator (Figure 3a). The high portion of nonflammable Al_2O_3 in the separator also helps reduce risks of thermal runaway.

The separator is prepared by dispersing ~10 μm Al_2O_3 particles (Sigma-Aldrich) and Poly(vinylidene fluoride-hexafluoropropylene) (PVdF-HFP) binders (Kynar 2801) in tetrahydrofuran (THF) for 12 hours and drop casting onto a flat glass substrate. The weight ratio of PVdF-HFP to Al_2O_3 varies from 1 : 4 to 1 : 9, corresponding to 1:1.8 to 1:4.1 in volume ratio. After drying, the Al_2O_3/PVdF-HFP film is peeled off from the glass substrate and pressed under 0.1 ton for 5 min. Figure 3b and c show optical and

SEM images of a typical sample. The size of granular Al_2O_3 particle is ~ 10 μm and it is wrapped by PVdF-HFP. The film thickness can be controlled between 30 μm and 200 μm by adjusting volume of dispersion dropped onto the glass substrate. Density data indicate that 50 - 60 % of the film is filled by Al_2O_3 and polymer, and the rest portion left is void (Table 2). The separator shows a reasonable ionic conductivity of 0.64-0.75 mS cm^{-1}, slightly lower than our measurements (0.88 mS cm^{-1}) and previous results[30] of commercial separators. We will show later that extra joule heating due to this slightly lower conductivity has negligible impact on the cell temperature rise.

The thermal conductivity of a dry composite separator is quite low, which are 0.17 ± 0.03, 0.22 ± 0.03 and 0.26 ± 0.04 W m^{-1} K^{-1} for samples with 80%, 85% and 90% of micro-Al_2O_3 (Figure 3d), respectively, as the thermal transport is mainly limited by the thermal contact resistance between particles, which is typically 10^{-4}-10^{-5} m^2 K W^{-1}, while the effective thermal resistance of an individual Al_2O_3 particle is much less, in the order of 10 μm / 35 W m^{-1} K^{-1} = 3 × 10^{-7} m^2 K W^{-1}. However, higher thermal conductivity is still observed in samples with large portion of Al_2O_3, suggesting the effectiveness of adding Al_2O_3 particles in enhancing thermal conductivity. After the composite film is saturated with DEC, its effective thermal conductivity (k_{eff}) dramatically increases to 0.71 ± 0.11, 0.83 ± 0.12, 1.13 ± 0.17 W m^{-1} K^{-1}, for micro-Al_2O_3/PVdF-HFP ratio of 80:20, 85:15 and 90:10, respectively, representing an enhancement of 4-5 X compared to dry samples (Figure 3d). The value is also 4-5X higher than commercial separators saturated with DEC as measured above (0.185 W m^{-1} K^{-1}). Although the sample with 90% Al_2O_3 meets the target of 1 W m^{-1} K^{-1}, the low content of PVdF-HFP inside indicates that the film may have a poor mechanical strength, especially under swelling condition with

electrolyte presented. Ideally separators should have both high thermal conductivity and reasonable polymer content to provide enough mechanical strength.

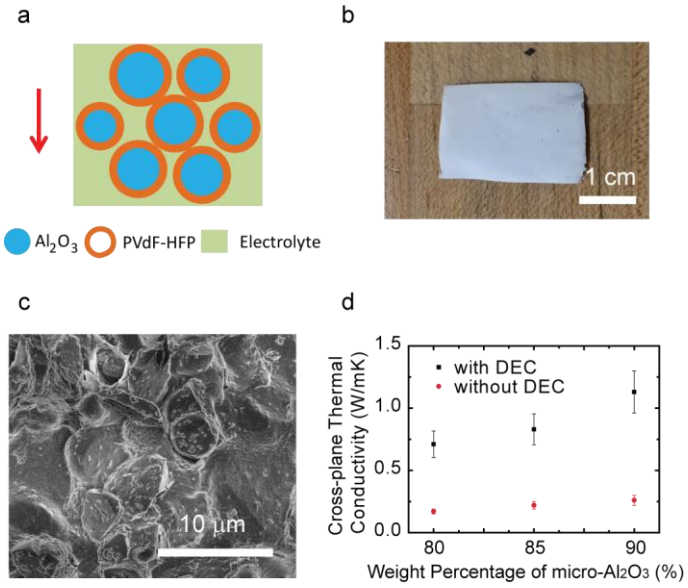

Figure 3. Micro-Al_2O_3/PVdF-HFP composite separator. a) A schematic of micro-Al_2O_3/PVdF-HFP composite to improve thermal conductivity of a separator. b) and c) Optical and SEM images of the composite separators. The particle size is ~ 10 μm. The weight ratio of micro-Al_2O_3 to PVdF-HFP is 85:15. d) Cross-plane thermal conductivity of the micro-Al_2O_3/PVdF-HFP separator.

Table 2. Properties of micro-Al_2O_3/PVdF-HFP and commercial separators

Al_2O_3: PVdF-HFP (weight)	80:20	85:15	90:10	Commercial PP/ PE/PP Separator
Density (g cm^{-3})	1.83	1.93	2.0	0.57
Volumetric Portion of Solid	0.58	0.58	0.56	0.61*
Ionic Conductivity (mS cm^{-1})	0.64	0.68	0.75	0.88
Thickness (μm)	30-200			25

*: based on porosity of 0.39

To increase thermal conductivity of the separator while maintaining a reasonable polymer content, we first try to understand why thermal conductivity of the composite separator (~ 1 W m^{-1} K^{-1}) is much lower than Al_2O_3 itself (~ 35 W m^{-1} K^{-1}). The heat transfer in the composite electrode is simplified as two polymer-wrapped Al_2O_3 spherical particles in contact with each other. COMSOL simulation shows that the thickness of polymer coating layer and thermal conductivity of the liquid phase are two dominant factors to impede heat transfer (figure 4b and c), while other factors, such as interfacial thermal conductance and contact area, have little effect on the effective thermal conductivity (figure S5). Based on simulation results, we proposed to replace certain amount of micron-sized Al_2O_3 (micro-Al_2O_3) particles with nanoparticles (nano-Al_2O_3) to address the two dominant factors discussed above. First, the large surface area of nanoparticles helps reduce the thickness of polymer layer on Al_2O_3 as polymer is assumed to be uniformly coated onto all Al_2O_3 particles. Second, nanoparticles could distribute in the gap among large Al_2O_3 particles to improve heat transfer in the DEC matrix.

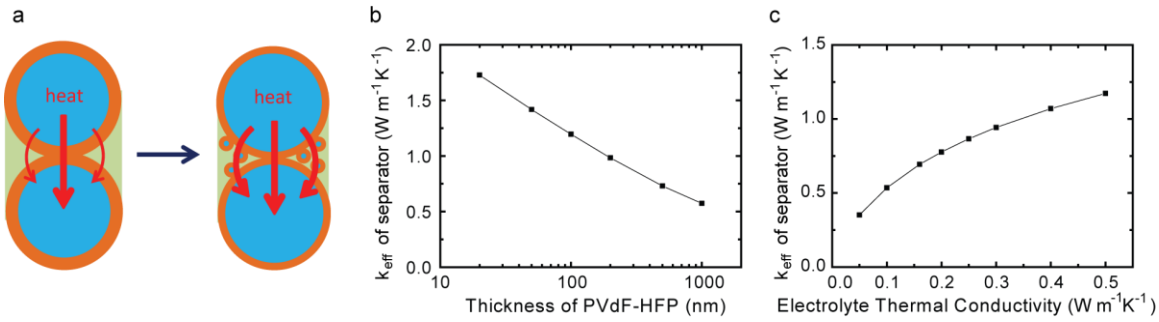

Figure 4. Thermally conductive separator with both nano- and micro-Al_2O_3. a) A conceptual schematic of adding Al_2O_3 nanoparticles to improve thermal conductivity. The addition of nanoparticles reduces thickness of polymer coating on micro-Al_2O_3 and enhances thermal

conductivity of the matrix. b) and c) Dependence of k_{eff} on b) the thickness of PVdF-HFP coating on Al_2O_3 particles, and c) *k* of electrolyte.

Based on the argument above, composite separators with 10 μm Al_2O_3, 100 nm Al_2O_3 and PVdF-HFP are prepared with the same procedure as samples without nano-Al_2O_3. The weight portion of PVdF-HFP is fixed to be 15 wt% (28.1 vol%) of all solids. The SEM image shows that Al_2O_3 nanoparticles distribute among micro-Al_2O_3 particles and they are glued by PVdF-HFP (figure S6b), which is similar with observations in composite battery electrodes[31]. Further analysis, such as 3D imaging by synchrotron, could help us understand the distribution and connectivity of particles in the composite. The ionic conductivity of samples with nano-Al_2O_3 is comparable to samples without nano-Al_2O_3, suggesting that the addition of nanoparticles does not apparently affect ionic transport (Table 3). Experimental results on thermal conductivity are illustrated in figure 4b. For dry samples, the thermal conductivity is basically the same as those without nano-Al_2O_3 in figure 3d, as the thermal transport is still limited by contact resistance. After saturating the composite with DEC, the thermal conductivity increases first as the content of nano-Al_2O_3 becomes higher, from 0.81 ± 0.12 W m^{-1} K^{-1} with 0 wt% nano-Al_2O_3 to 1.05 ± 0.16 W m^{-1} K^{-1} with 15 wt% nano-Al_2O_3, which is consistent with our prediction and meets the goal of 1 W m^{-1} K^{-1}. However, the thermal conductivity drops down when the content of nano-Al_2O_3 is over 20 wt% in the solid phase. This may arise from the fact that micro-Al_2O_3 particles are separated by nano-Al_2O_3 particles and they no longer form a network to efficiently conduct heat at low portion of micro-Al_2O_3.

Table 3. Properties of nano/micro-Al_2O_3/PVdF-HFP composite separator

Micro-Al_2O_3: nano-Al_2O_3 (weight)	65:20	70:15	75:10	80:5	85:0
Density (g cm^{-3})	1.70	1.74	1.85	1.88	1.93
Volumetric Portion of Solid in the separator	0.51	0.52	0.55	0.59	0.6
Ionic Conductivity (mS cm^{-1})	0.74	0.69	0.75	0.67	0.68

To better understand thermal transport in the composite and help future development, we use effective medium theory to model the dependence of k_{eff} on separator composition. The Bruggeman's model with spherical inclusion is used here and it is applied to micro-Al_2O_3/PVdF-HFP separator saturated with DEC first. The Bruggeman's model[32] indicates that

$$\sum \lambda_i \frac{k_i - k_{eff}}{k_i + 2k_{eff}} = 0 \qquad (1)$$

where λ is the volume portion and subscript *i* means different phases in the composite. As PVdF-HFP is coated onto Al_2O_3 particles, two phases exist: PVdF-HFP wrapped Al_2O_3 and DEC. The effective thermal conductivity of a PVdF-HFP wrapped Al_2O_3 particle ($k_{Al2O3,polymer}$)) is calculated based on following assumptions and approximations: 1) all PVdF-HFP is uniformly coated onto Al_2O_3 particles and the shape of Al_2O_3 particle is spherical. 2) The thermal resistance of the particle is that of Al_2O_3 and PVdF-HFP in series. Interfacial thermal resistance between DEC and solid is neglected as it is typically much smaller than thermal resistances of micro-Al_2O_3 particles (10^{-7} - 10^{-8} m^2 K W^{-1} vs. 10^{-6} -10^{-4} m^2 K W^{-1})[29]. *k* used in calculations are 35 W m^{-1} K^{-1} for micro-Al_2O_3, 0.19 W m^{-1} K^{-1} for PVdF-HFP and 0.16 W m^{-1} K^{-1} for DEC[33].

k_{eff} of the micro-Al_2O_3/PVdF-HFP composite separator predicted by the Bruggeman's model fits well with experimental results (figure 5a). We further apply the model to calculate k_{eff} of nano/micro-Al_2O_3/PVdF-HFP composite. In such a composite, three phases exists: PVdF-HFP wrapped micro-Al_2O_3, PVdF-HFP wrapped nano-Al_2O_3 and DEC. Besides assumptions used in the micro-Al_2O_3/PVdF-HFP composite above, the thickness of PVdF-HFP on both micro-Al_2O_3 and nano-Al_2O_3 are assumed to be the same, and k of nano-Al_2O_3 is supposed to be 12 W m^{-1} K^{-1} to take size-dependent thermal conductivity into account[29]. However, the predicted values are 50%-100% higher than experimental results (figure 5b). This suggests that the assumption of uniform coating of PVdF-HFP on both nano-Al_2O_3 and micro-Al_2O_3 may not be valid. It is well known that nanoparticles tend to agglomerate due to strong interaction among themselves. Therefore it is speculated that there is less PVdF-HFP on nano-Al_2O_3 than the well dispersed situation; thus the thickness of PVdF-HFP on micro-Al_2O_3 is larger than that in uniform coating, which gives a lower k_{eff} than the prediction. The higher k_{eff} predicted by the model also implies that further optimization of particle dispersion and polymer coating may boost k_{eff} to ~ 2 W m^{-1} K^{-1}.

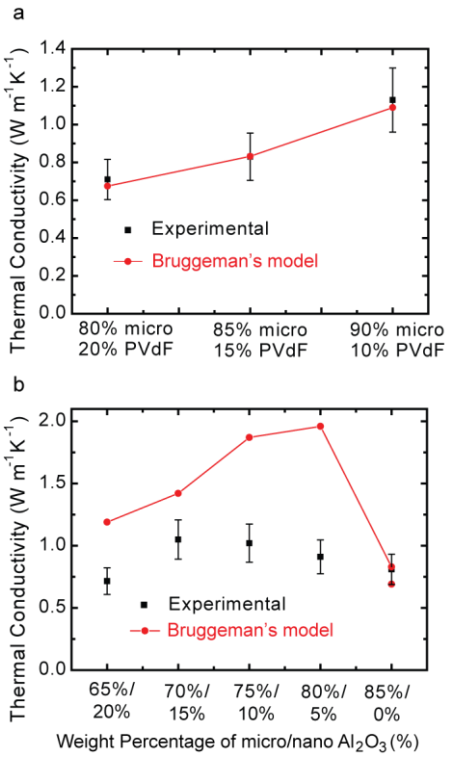

Figure 5. k_{eff} of the composite separator calculated by the Bruggeman's model. a) Micro-Al_2O_3/PVdF-HFP composite separators. b) Nano/micro-Al_2O_3/PVdF-HFP composite separators. The weight percentage of PVdF-HFP is fixed as 15%.

A concern in applying Al_2O_3/polymer separator to enhance heat dissipation is that whether the lower ionic conductivity of Al_2O_3/polymer separator increases heat generation in batteries and thus compensates its higher thermal conductivity. Table 2 and 3 show that the ionic conductivity of Al_2O_3/polymer is ~0.2 mS cm^{-1} lower than commercial separators. Let us use 18650 cell as an example. The typical thickness and size of separator in a 18650 cell are 25 μm and 6 × 50 cm^2, respectively, it is estimated that the extra overpotential due to lower ionic conductivity is ~ 25 mV at 3 C rate, which is only 4% of the total overpotential of ~0.6 V and has little effect on heat generation. COMSOL simulations show that this extra overpotential only causes an extra temperature

rise of 0.27 K, which is only 12% of the temperature reduction due to enhanced thermal conductivity of separator (2.16 K). Similarly, this extra overpotential results in an extra temperature rise of 1.1 K for four-prismatic-cell pack discussed above, which corresponds to only 8.5% of the temperature reduction due to enhanced thermal conductivity of separator (12.9 K). Moreover, as the porosity of Al_2O_3/polymer separators is similar to that of commercial ones, we believe that ionic conductivity of such composite separators can be further improved. Another concern is the mechanical strength of the separator when it is soaked in electrolyte, as the organic electrolyte in Li-ion batteries could swell the separator. This issue could be addressed by replacing PVdF-HFP with other polymers with better mechanical properties, such as polyvinyl alcohol.

The stability of such composite separator is also tested by attaching it to a lithium metal and soak in electrolyte (1 M $LiPF_6$ in EC/DEC) for seven days. XRD data don't show any new peaks, and there is no obvious change in camera images (figure 6). These results indicate that no or only trace amount of Al_2O_3 has reacted with lithium. We believe that the polymer coating layer on Al_2O_3 avoids the direct contact between Al_2O_3 and lithium. As a result, the degree of reaction is very limited and it should have little impact on thermal conductivity of the whole composite. Further investigation is needed to evaluate the long term stability of such composite separator.

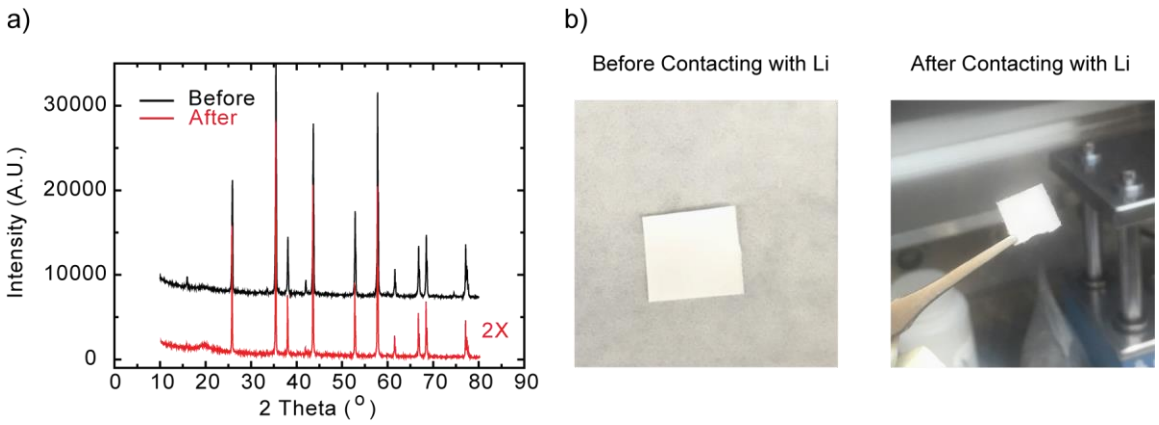

Figure 6. Stability of Al_2O_3/polymer separator against lithium metal. The composite separator is attached to lithium and soaked in 1M LiPF6 in EC/DEC for seven days. (a) XRD pattern before and after contacting with Li. (b) Optical image of a composite separator before and after contacting with Li. No change has been observed. It is supposed that polymer coating effectively block direct reaction between lithium and Al_2O_3.

3. Conclusion

In summary, $k_{\perp}$ of battery separator is important to thermal management of batteries. A nano/micro-Al_2O_3/PVdF-HFP-based composite separator is developed with high thermal conductivity (~1 W m^{-1} K^{-1}), which is ~5 times that of common PE-based separators. The addition of Al_2O_3 nanoparticles helps further enhance thermal conductivity of the composite. The mechanism is assumed to be that Al_2O_3 nanoparticles help reduce thickness of polymer coating on micro-Al_2O_3 and improve effective thermal conductivity of the electrolyte. Such thermally conductive separator could have potential applications to dissipate heat faster in batteries and reduce temperature rise in operation, especially under external forced liquid cooling.

List of Symbols

A: Cross-section area of a sample, or a battery, surface area for convection

h: Heat transfer coefficient

k: Thermal Conductivity of the sample (W $m^{-1}K^{-1}$)

$k_{\perp}$: Cross-plane thermal conductivity of a battery component with DEC (W $m^{-1}K^{-1}$)

$k_{//}$: In-plane thermal conductivity of a battery component with DEC (W $m^{-1}K^{-1}$)

$k_{Al2O3,polymer}$: The effective thermal conductivity of an Al_2O_3 particle coated with PVdF-HFP (W $m^{-1}K^{-1}$)

k_{eff}: Effective thermal conductivity of an Al_2O_3/polymer composite with DEC (W $m^{-1}K^{-1}$)

$k_{\perp,separator}$: Cross-plane thermal conductivity of a separator (W $m^{-1}K^{-1}$)

l: Heat transport distance

T_{rise}: temperature rise due to heating inside batteries

Δx: Thickness of the sample (m)

λ: Volume portion of a certain phase

Acknowledgment: We would like to thank Daniel Kraemer for developing the differential steady-state method to measure thermal conductivity and helpful discussions. This material is based upon work supported as part of the Solid State Solar-Thermal Energy Conversion Center (S^3TEC), an Energy Frontier Research Center funded by the U.S. Department of Energy, Office of Science, Office of Basic Energy Sciences under Award Number DE-SC0001299/DE-FG02-09ER46577. Yuan Yang thanks support from startup funding from Columbia University.

References

1. Armand, M.; Tarascon, J.-M. *Nature* 451 (2008), 652-657.
2. Whittingham, M. S. *Chemical Reviews* 104 (2004), 4271-4301.
3. Al Hallaj, S.; Maleki, H.; Hong, J. S.; Selman, J. R. *Journal of Power Sources* 83 (1999), 1-8.
4. Bandhauer, T. M.; Garimella, S.; Fuller, T. F. *Journal of the Electrochemical Society* 158 (2011), R1-R25.
5. Gu, W. B.; Wang, C. Y., *Thermal-electrochemical coupled modeling of a lithium-ion cell*. 2000; Vol. 99, p 748-762.
6. Ramadesigan, V.; Northrop, P. W. C.; De, S.; Santhanagopalan, S.; Braatz, R. D.; Subramanian, V. R. *Journal of the Electrochemical Society* 159 (2012), R31-R45.
7. Chiu, K.-C.; Lin, C.-H.; Yeh, S.-F.; Lin, Y.-H.; Chen, K.-C. *Journal of Power Sources* 251 (2014), 254-263.
8. Kim, G.-H.; Pesaran, A.; Spotnitz, R. *Journal of Power Sources* 170 (2007), 476-489.
9. Wang, Q.; Ping, P.; Zhao, X.; Chu, G.; Sun, J.; Chen, C. *Journal of Power Sources* 208 (2012), 210-224.
10. Luo, W.; Zhou, L.; Fu, K.; Yang, Z.; Wan, J.; Manno, M.; Yao, Y.; Zhu, H.; Yang, B.; Hu, L. *Nano Letters* 15 (2015), 6149-6154.
11. Baker, D. R.; Verbrugge, M. W. *Journal of the Electrochemical Society* 146 (1999), 2413-2424.
12. Fan, L.; Khodadadi, J. M.; Pesaran, A. A. *Journal of Power Sources* 238 (2013), 301-312.
13. Kizilel, R.; Sabbah, R.; Selman, J. R.; Al-Hallaj, S. *Journal of Power Sources* 194 (2009), 1105-1112.
14. Mottard, J. M.; Hannay, C.; Winandy, E. L. *Journal of Power Sources* 117 (2003), 212-222.
15. Ji, Y.; Wang, C. Y. *Electrochimica Acta* 107 (2013), 664-674.
16. Fang, W.; Kwon, O. J.; Wang, C.-Y. *International Journal of Energy Research* 34 (2010), 107-115.
17. Cai, L.; White, R. E. *Journal of the Electrochemical Society* 157 (2010), A1188-A1195.
18. Wu, B.; Yufit, V.; Marinescu, M.; Offer, G. J.; Martinez-Botas, R. F.; Brandon, N. P. *Journal of Power Sources* 243 (2013), 544-554.
19. Xun, J.; Liu, R.; Jiao, K. *Journal of Power Sources* 233 (2013), 47-61.
20. Huang, X. *Journal of Solid State Electrochemistry* 15 (2011), 649-662.
21. Xiao, M.; Choe, S.-Y. *Journal of Power Sources* 241 (2013), 46-55.
22. Maleki, H.; Al Hallaj, S.; Selman, J. R.; Dinwiddie, R. B.; Wang, H. *Journal of the Electrochemical Society* 146 (1999), 947-954.
23. Kraemer, D.; Chen, G. *Review of Scientific Instruments* 85 (2014).
24. Abdulagatov, I. M.; Azizov, N. D. *International Journal of Thermophysics* 26 (2005), 593-635.
25. John H. Lienhard V; IV, J. H. L., *A Heat Transfer Textbook*. 2011, 2011.
26. http://www.hybridautocenter.com/HAC4/index.php?option=com_hikashop&ctrl=product&task=show&cid=3&name=nissan-leaf-battery-module-model-2012-new&Itemid=605
27. John H. Lienhard iv; v, J. H. L., *A Heat Transfer Textbook*. Phlogiston Press: 2015.
28. Shen, S.; Henry, A.; Tong, J.; Zheng, R.; Chen, G. *Nature Nanotechnology* 5 (2010), 251-255.
29. Minnich, A. J. Exploring Electron and Phonon Transport at the Nanoscale for Thermoelectric Energy Conversion. MIT, 2011.
30. Lee, Y. M.; Seo, J. E.; Choi, N. S.; Park, J. K. *Electrochimica Acta* 50 (2005), 2843-2848.

31. Liu, G.; Zheng, H.; Song, X.; Battaglia, V. S. *Journal of the Electrochemical Society* 159 (2012), A214-A221.
32. Bruggeman, D. A. G. *Annalen Der Physik* 24 (1935), 636-664.
33. Jin, X. G.; Wu, J. T.; Liu, Z. G.; Pan, J. *Fluid Phase Equilibria* 220 (2004), 37-40.